

Ferroelectricity and piezoelectricity in monolayers and nanoplatelets of SnS

Alexander I. Lebedev^{1, a)}

Physics Department, Moscow State University, 119991 Moscow, Russia

(Dated: 30 October 2018)

The ground-state structure of monolayers and nanoplatelets of SnS with a thickness from two to five monolayers is calculated from first principles. It is shown that nanoobjects with only odd number of monolayers are ferroelectric. The ferroelectric, piezoelectric, and elastic properties of these polar structures are calculated. The appearance of polarization in these nanoobjects is explained by an uncompensated polarization that exists in an antiferroelectric structure of bulk SnS. The mechanism of ferroelectricity, in which the ferroelectric distortion is associated with short-range ordering of lone pairs, can be regarded as a way of creating ferroelectrics with high Curie temperature.

PACS numbers: 62.23.Kn, 68.65.-k, 77.84.-s, 81.07.Bc

I. INTRODUCTION

In recent years, quasi-two-dimensional (2D) structures—monolayers and nanoplatelets with a thickness of a few monolayers—have gained a considerable attention.^{1–4} These structures have demonstrated many interesting properties which differ much from those of bulk crystals. Tin sulfide SnS, which in the bulk form is a semiconductor with a layered structure, can be split into monolayers and nanoplatelets by chemical methods.^{5–7} The interest to SnS quasi-2D structures is stimulated by their thermoelectric, electric, and optical properties^{8–17} and the predicted ferroelectricity in SnS monolayers.^{18,19} The latter suggests a possible application of piezoelectric properties of these structures. As concerns to SnS nanoplatelets containing more than one monolayer, only the optical properties of these nanoobjects have been studied.^{7,8,10}

At room temperature, SnS crystallizes in the *Pnma* structure. At 878 K, it undergoes a second-order structural phase transition into a high-temperature *Cmcm* phase.²⁰ This phase has a distorted NaCl structure and consists of two-layer slabs of this structure which are shifted against the adjacent slabs by a half of the translation vector of the NaCl structure [Fig. 1(a)]. The chemical bonding between the slabs is believed to be of van der Waals type; such structures can be easily split into the slabs (monolayers). The *Fm $\bar{3}$ m* structure of SnS is another metastable phase which was obtained in epitaxial films.²¹

The use of GGA-PBE PAW pseudopotentials in earlier first-principles calculations of SnS nanostructures^{11,13,14,18,22} resulted in the unit cell volume of bulk *Pnma* phase, which strongly (by $\sim 6\%$) exceeded the experimental one. This can lead to an overestimation of the ferroelectric instability and other ferroelectric properties. Our tests have shown that the local density approximation (LDA) PAW pseudopotentials underestimate the unit cell volume by 6.2% and the energies of

the ferroelectric ordering in SnS monolayers calculated using the GGA and LDA functionals differ by more than 40 times.²³ On the other hand, the applicability of the GGA functional to two-dimensional systems is questionable because of an inaccuracy in its correlation part. For these systems, the LDA approximation usually gives better results.²⁴ In this work, we used norm-conserving LDA pseudopotentials, for which the unit cell volume of bulk SnS is underestimated by only $\sim 1\%$ against the experimental data extrapolated to $T = 0$. In addition to the studies of ferroelectric and piezoelectric properties of SnS monolayers, in this work the ground-state structure and properties of SnS nanoplatelets with a thickness from 2 to 5 monolayers (MLs) are calculated and the origin of “intermittent” ferroelectricity revealed in these nanoplatelets is discussed.

II. CALCULATION TECHNIQUE

The first-principles calculations presented in this work were carried out within the density functional theory using the ABINIT software package and norm-conserving pseudopotentials constructed using the RKKJ scheme²⁵ in the local density approximation.²⁶ The cutoff energy was 30 Ha (816 eV) and the integration over the Brillouin zone was performed using an $8 \times 8 \times 4$ Monkhorst–Pack mesh. Equilibrium lattice parameters and atomic positions were obtained by relaxing the forces acting on the atoms to a value below $2 \cdot 10^{-6}$ Ha/Bohr (0.1 meV/Å). The phonon spectra and the elastic and piezoelectric moduli were calculated using the density-functional perturbation theory. The Berry phase method was used to calculate the polarization.

III. RESULTS

A. Phase relations for bulk SnS

The calculation of the energies of different possible structures of bulk SnS shows that the *Pnma* structure

^{a)}swan@scon155.phys.msu.ru

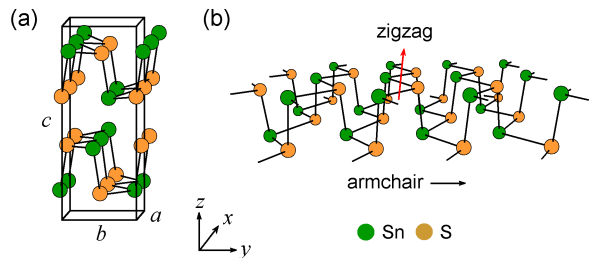


FIG. 1. Structures of (a) bulk SnS and (b) SnS monolayer.

is the ground-state structure, in agreement with experiment. The energies of the $Cmcm$ and $Fm\bar{3}m$ phases are by 20 and 49 meV per formula unit higher than that of the $Pnma$ phase. The calculation of the phonon spectra and elastic tensors for these phases shows that the $Fm\bar{3}m$ and $Pnma$ phases fulfill the stability criterion, i.e., all optical phonon frequencies in the Brillouin zone in them are positive and their structures are mechanically stable. This suggests that the $Fm\bar{3}m$ phase which has a higher energy is metastable. As concerns to the $Cmcm$ phase, two instabilities are observed in its phonon spectrum: the ferroelectric one at the center of the Brillouin zone (the phonon frequency is $63i \text{ cm}^{-1}$) and another one at the Y point on its boundary (the phonon frequency is $35i \text{ cm}^{-1}$). The ferroelectric instability results in a phase transition to a metastable $Cmc2_1$ phase whose energy is by 15.5 meV higher than that of the $Pnma$ phase. The condensation of the unstable phonon at the Y point transforms the structure into the ground-state $Pnma$ phase. These two instabilities in the $Cmcm$ phase compete with each other; the appearance of structural distortions described by the unstable phonon at the Y point suppresses the ferroelectric instability.²⁷

A tendency of the SnS structure to be split into separate monolayers when stretching it along the z axis is illustrated by a divergence of the S_{33} component of the elastic compliance tensor of the $Pnma$ phase at a certain critical pressure p_c . This pressure can be determined as a maximum internal pressure in the unit cell, which can be obtained by changing the c lattice parameter when relaxing atomic positions and two other lattice parameters. The calculations show that $p_c = 28.2$ kbar for the $Pnma$ phase. The splitting of the metastable $Fm\bar{3}m$ phase is a more complicated process because the stretched sample (whose symmetry decreases to $I4/mmm$ under strain) exhibits a ferroelectric phase transition at 10.1 kbar and then a first-order phase transition to the $P4/nmm$ phase. The p_c value for this phase is 25 kbar.

B. Phase relations for SnS monolayers

To determine the ground-state structure of SnS monolayers and calculate their physical properties, the super-

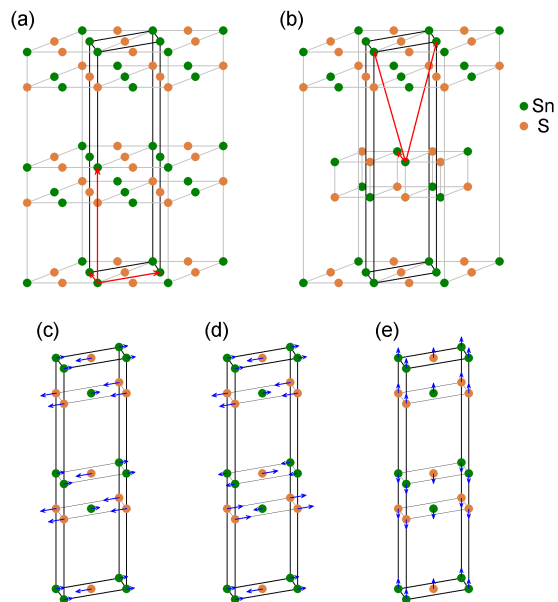


FIG. 2. [(a), (b)] The supercells used to study the properties of SnS monolayers. The translation vectors of the (a) $P4/nmm$ and (b) $Cmcm$ primitive units cells are shown by red lines. The eigenvectors of (c) E_u , (d) Z_5^- , and (e) Z_1^- unstable modes found in the $P4/nmm$ structure.

cells obtained by strong stretching of the $Fm\bar{3}m$, $Cmcm$, and $Pnma$ structures of bulk SnS along the z axis were considered. As the ABINIT program requires the optimizable translation vectors to be orthogonal to the translation vector that is fixed, supercells containing four formula units were used for $Fm\bar{3}m$ and $Cmcm$ structures [Figs. 2(a) and 2(b)]. The stretching of the supercells results in appearance of two monolayers separated by vacuum gaps. After splitting, the symmetry of the $Fm\bar{3}m$ supercell is reduced to $P4/nmm$, whereas the $Cmcm$ and $Pnma$ supercells retain their symmetry. When increasing the c lattice parameter, the difference between the a and b lattice parameters in the $Cmcm$ supercell becomes very small ($<0.0001 \text{ \AA}$ at $c = 26.46 \text{ \AA}$). The comparison of the evolution of these supercells will help us later to reveal different properties of nanoplatelets prepared from monolayers conjugated at the interface by different ways.

An increase in the thickness of the vacuum gap changes the energies of the discussed supercells. For supercells containing two monolayers, these changes saturate above $c = 25.4 \text{ \AA}$. This suggests that the thickness of the vacuum gap of $\sim 9.5 \text{ \AA}$ is sufficient to neglect the interaction between monolayers. When increasing c , the energy difference between the $P4/nmm$ and $Cmcm$ phases abruptly decreases, but the energy of the $Pnma$ phase remains lower (Table I). The weakness of the interaction between monolayers is confirmed by the low residual pressure in the supercells. At $c = 26.46 \text{ \AA}$ it is 0.04 kbar, which is about three orders of magnitude lower than the

TABLE I. Energies of different phases of SnS monolayers (in meV per primitive unit cell). The energy of the $P4/nmm$ phase is taken as the energy origin.

Phase	Displacement direction	c (Å)			
		18.52	21.17	26.46	31.75
$P4/nmm$	—	0	0	0	0
$Cmcm$	—	-0.204	+0.002	+0.001	+0.001
$P2_1/c$	[110]	-0.984 ^a	-0.766 ^a	-0.752	-0.757
$Cmca$	[110]	-0.759	-0.771	-0.753	-0.756
$Abm2$	[110]	-0.787	-0.786	-0.760	-0.743
Cc	[110]	-0.968	-0.797	-0.765	-0.766
$Pmn2_1$	[100],[010]	-1.361	-1.336	-1.320	-1.304
$Ama2$	[010]	-1.539	-1.351	-1.320	-1.310
$Cmc2_1$	[100]	-1.540	-1.350	-1.320	-1.310
$Pnmm$	[100]	-1.521	-1.347	-1.323	-1.312
$Pnma$	[010]	-1.559	-1.347	-1.322	-1.314

^a This phase is unstable against its transformation into the $Pnma$ or $Pnmm$ phase in supercells with small vacuum gaps. At large vacuum gaps, it becomes more stable. The reported energies were calculated for the case of $P_x \approx P_y$ (the condition that is satisfied at large vacuum gaps).

critical pressure p_c .

The calculations of the phonon spectra were performed using primitive unit cells extracted from the supercells. The calculations for a SnS monolayer modeled with the $P4/nmm$ supercell find a doubly degenerate unstable ferroelectric E_u mode with a frequency of $37i$ cm^{-1} at the Γ point and two unstable modes at the Z point of the Brillouin zone [Fig. 3(a)]:²⁸ a doubly degenerate antiferroelectric Z_5^- mode and a weak nondegenerate Z_1^- mode with a frequency of $0.199i$ cm^{-1} describing an acoustic-like antiparallel shift of adjacent monolayers along the z axis. The eigenvectors of these modes are shown in Figs. 2(c)–2(e). The latter mode describes the coalescence of monolayers into a nanoplatelet, and this is why it will be called hereafter the coalescence mode. In several cases, a very weak ($\sim 0.03i$ cm^{-1}) unstable doubly degenerate mode describing an acoustic-like antiparallel sliding of adjacent monolayers in the xy plane appeared in the spectrum. The frequency of the antiferroelectric Z_5^- mode, in which the polar atomic displacements in the xy plane in adjacent monolayers are antiparallel to each other, differs from the frequency of the ferroelectric E_u mode by less than 0.001 cm^{-1} . This indicates a weak interaction between polarizations in adjacent monolayers.

The comparison of the energies of two possible $Abm2$ and $Pmn2_1$ polar phases, into which the $P4/nmm$ structure can transform upon the ferroelectric distortion, shows that the energy of the $Pmn2_1$ phase is lower (Table I). An analysis of the phonon spectra and elastic tensors of these two phases shows that the $Abm2$ phase is unstable, whereas the $Pmn2_1$ phase meets the stability criterion except for weak unstable modes at the Z point resulting from a weak interaction between the monolayer

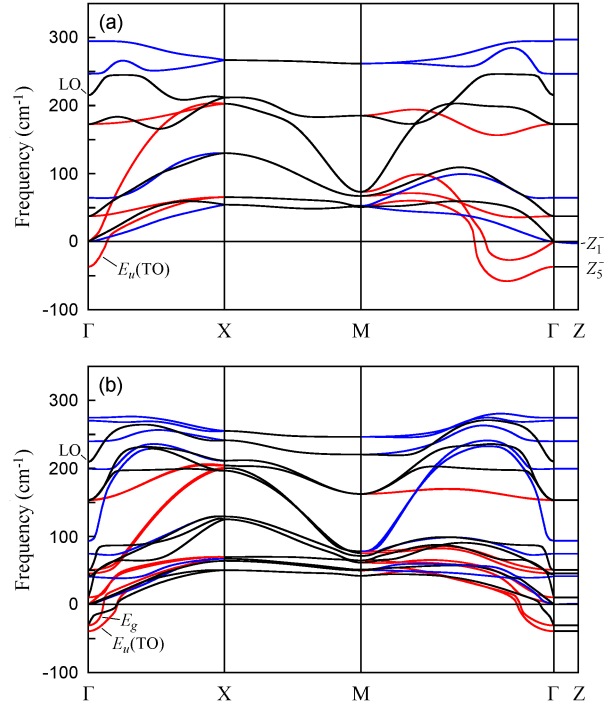


FIG. 3. Phonon spectra of nanoplatelets with a thickness of (a) 1ML and (b) 2ML and the $P4/nmm$ structure. Calculations were performed on supercells with the c lattice parameter of 15.88 Å and 21.17 Å, respectively. Because of a strong intermixing of longitudinal and out-of-plane atomic displacements, the polarization of modes is well defined only near the Γ point. The red lines are transverse modes with in-plane polarization, the blue lines are transverse modes with out-of-plane polarization, and the black lines are longitudinal modes.

and its images. The condensation of the unstable antiferroelectric Z_5^- mode can result in appearance of the $Cmca$ and $Pnma$ phases. The $Cmca$ phase is unstable and relaxes to the $Pnma$ phase or to a metastable $Abm2$ phase, in which the polarization in adjacent monolayers is rotated by $\sim 90^\circ$.

The calculations of the phonon spectrum of a SnS monolayer modeled with the $Cmcm$ supercell find two unstable ferroelectric modes, B_{2u} and B_{3u} , with close energies at the Γ point ($37i$ cm^{-1}) and at least three unstable modes at the Y point. These are two antiferroelectric modes whose frequencies are very close to those of the ferroelectric modes and a weak coalescence mode ($0.197i$ cm^{-1}). In several cases, one or two very weak ($\sim 0.03i$ cm^{-1}) unstable modes describing an antiparallel sliding of adjacent monolayers in the xy plane appeared in the spectrum. An analysis of properties of three possible $Cmc2_1$, $Ama2$, and Cc polar phases, into which the $Cmcm$ structure can transform upon the ferroelectric distortion, shows that the Cc phase is unstable and the $Cmc2_1$ and $Ama2$ phases have the same lowest

energy (Table I). The coincidence in their energies is a result of nearly equal a and b lattice parameters in the $Cmcm$ supercell. The condensation of unstable antiferroelectric modes can result in appearance of the $Pnmm$, $P2_1/c$, and $Pnma$ phases. The $P2_1/c$ phase is unstable, and the $Pnmm$ and $Pnma$ phases have close lowest energies.

The comparison of the energies of all found phases (Table I) shows that among possible ground-state structures of SnS monolayers, the phases with the [100] or [010] atomic displacements are the most energetically favorable. The weak dependence on the direction results from close a and b lattice parameters in the parent structures. However, the result why the energy is nearly independent on whether the supercell structure is ferroelectric or antiferroelectric needs explanation.

This result is not surprising since in the $c \rightarrow \infty$ limit all found solutions are physically equivalent and differ only by the orientation of polarization in weakly interacting adjacent monolayers. The appearance of the non-polar $Pnma$ and $Pnmm$ phases does not contradict the polar $Cmc2_1$, $Ama2$, and $Pmn2_1$ solutions because in the $Pnma$ and $Pnmm$ structures there are glide planes reversing the x or y direction of polarization upon a half-period shift along the z axis. This means that the $Pnma$ and $Pnmm$ structures are actually *antiferroelectric*. Taking into account that the $Ama2$ and $Cmc2_1$ phases differ only by the polarization direction and the $Cmc2_1$ and $Pmn2_1$ phases have the same polarization direction and differ by the way of conjugation of adjacent monolayers, in the $c \rightarrow \infty$ limit these differences become negligible, and the $Pmn2_1$ phase can be considered as the ground-state structure of SnS monolayers. The polarization in this structure is directed along the armchair direction [Fig. 1(b)]. Our conclusion agrees with the results of earlier calculations,^{9,14} but disagrees with the $Pm\bar{c}n$ space group incorrectly identified in Ref. 13 (this group is non-polar).

C. Coalescence of monolayers and properties of SnS nanoplatelets

As noted above, in the phonon spectra of all studied SnS supercells there is a weak unstable mode whose eigenvector describes the coalescence of the monolayers into a two-layer (2ML) nanoplatelet. The typical frequency of this mode is $0.2\text{--}2i$ cm^{-1} for both $P4/nmm$ and $Cmcm$ supercells.

The coalescence of SnS monolayers into the 2ML nanoplatelet is indeed energetically favorable. The energy gain, however, depends on how the monolayers are conjugated at the interface. For nanoplatelets with the $Pm\bar{c}n$ symmetry, which are obtained from the $Cmcm$ supercell, the energy gain is notably higher than for nanoplatelets with the $P4/nmm$ symmetry obtained from the $P4/nmm$ supercell (Table II). We note that both energy gains are too high to explain the chemical

TABLE II. Energies of different phases of 2ML SnS nanoplatelets obtained from the $P4/nmm$ and $Pm\bar{c}n$ parent structures. The energy of two isolated monolayers is taken as the energy origin. The energy of the most stable phase is in boldface.

Phase	Unstable phonon and order parameter	Displacement direction	Energy (meV/2ML)
$P4/nmm$	—	—	−295.8
$Abm2$	$E_u(\eta, \eta)$	[110]	−297.3
$Pmn2_1$	$E_u(\eta, 0)$	[100]	−298.6
$C2/m$	$E_g(\eta, \eta)$	[110]	−371.8
$P2_1/m$	$E_g(\eta, 0)$	[100]	−483.6
$Pm\bar{c}n$	—	—	−455.1
$Pma2$	B_{2u}	[010]	−455.2
$Pmc2_1$	B_{3u}	[100]	−464.7
$P2_1/m$	B_{2g}	[010]	− 483.7

bonding between monolayers by van der Waals (vdW) interaction only: typical bonding energies for vdW systems is one order of magnitude smaller.²⁹ Large energy gains mean that the nanoplatelet/monolayer surfaces need a coating to protect them against the aggregation.

The phonon spectrum of a SnS 2ML nanoplatelet with the $P4/nmm$ symmetry exhibits two doubly degenerate unstable modes at the Γ point [Fig. 3(b)]: the ferroelectric E_u mode ($39i$ cm^{-1}) and the antiferroelectric E_g mode ($31i$ cm^{-1}), which differ by the orientation of polarization in adjacent monolayers.

The phonon spectrum of a SnS 2ML nanoplatelet with the $Pm\bar{c}n$ symmetry exhibits three unstable modes at the Γ point: a strong ferroelectric B_{3u} mode ($52i$ cm^{-1}) polarized along the zigzag direction (with transition to the $Pmc2_1$ phase), a weak ferroelectric B_{2u} mode ($8i$ cm^{-1}) polarized along the armchair direction (with transition to the $Pma2$ phase), and a B_{2g} mode ($31i$ cm^{-1}) describing strong antiferroelectric atomic displacements along the armchair direction (with transition to the $P2_1/m$ phase). The energy gain resulting from the latter distortion (28.6 meV per unit cell) is much higher than those for both ferroelectric distortions.

As follows from Table II, among the phases resulting from condensation of the unstable modes, the $P2_1/m$ ones have the lowest energy. The energy of the phase obtained from the $P4/nmm$ parent structure is slightly higher than the energy of the same phase obtained from the $Pm\bar{c}n$ parent structure. Taking into account that these phases are nearly the same and the difference in their energies results from different interaction between the nanoplatelet and its images, one can conclude that the ground-state structure of the 2ML nanoplatelet is $P2_1/m$, and so these nanoplatelets are not ferroelectric.³⁰ The structures of the ground state of nanoplatelets with different thickness are given in the supplementary material.

Surprisingly, the search for the ground-state structure

TABLE III. Energies of different phases of 3ML SnS nanoplatelets obtained from the $P4/nmm$ and $Pmnm$ parent structures. The energy of three isolated monolayers is taken as the energy origin. The energy of the most stable phase is in boldface.

Phase	Unstable phonon and order parameter	Displacement direction	Energy (meV/3ML)
$P4/nmm$	—	—	-639.2
$C2/m$	$E_g(\eta, \eta)$	[110]	-739.0
$Abm2$	$E_u(\eta, \eta)$	[110]	-760.1
$P2_1/m$	$E_g(\eta, 0)$	[100]	-933.1
$Pmn2_1$	$E_u(\eta, 0)$	[100]	-971.9
$Pmnm$	—	—	-905.8
$P2_1/m$	B_{3g}	[100]	-908.9
$Pmn2_1$	B_{3u}	[100]	-924.7
$P2_1/m$	B_{2g}	[010]	-933.2
$Pmn2_1$	B_{2u}	[010]	-971.9

of three-layer (3ML) SnS nanoplatelets reveals that they become ferroelectric again. The phonon spectrum of the $Pmnm$ phase exhibits four nondegenerate unstable modes at the Γ point, whereas the phonon spectrum of the $P4/nmm$ phase exhibits four doubly degenerate unstable modes (two ferroelectric E_u and two antiferroelectric E_g modes). As the eigenvectors of the unstable phonon modes become very complicated, the comparison of the energies of the different low-symmetry phases turns out to be more informative. The comparison of the energies of nanoplatelets conjugated in different ways (Table III) shows that the $Pmnm$ parent structure obtained using the $Cmcm$ conjugation scheme is energetically more favorable as compared to the $P4/nmm$ parent structure. The ground-state structure of the 3ML nanoplatelet is the polar $Pmn2_1$ phase polarized along the armchair direction (see also Fig. 4).

The study of four-layer (4ML) SnS nanoplatelets reveals that the $Pmma$ phase obtained using the $Cmcm$ conjugation scheme is the lowest-energy parent structure (Table IV). The phonon spectrum of this phase exhibits six nondegenerate unstable modes at the Γ point, whereas the phonon spectrum of the $P4/nmm$ phase exhibits four doubly degenerate unstable modes at the Γ point (ferroelectric E_u and antiferroelectric E_g modes). It should be noted that phonon spectra of this and thicker nanoplatelets exhibit several modes with same symmetry, but with different displacement patterns. In this case, the structural optimization usually gives the energy of the lowest-energy phase and the calculation of the “excited states” needs additional cumbersome orthogonalization procedure. This is why only the data for these low-energy phases are presented in Tables IV and V. The ground-state structure of the 4ML SnS nanoplatelet (the $P2_1/m$ phase) is not ferroelectric.

The study of five-layer (5ML) SnS nanoplatelets reveals that phonon spectra of parent $P4/nmm$ and $Pmnm$

TABLE IV. Energies of different phases of 4ML SnS nanoplatelets obtained from the $P4/nmm$ and $Pmma$ parent structures. The energy of four isolated monolayers is taken as the energy origin. The energy of the most stable phase is in boldface.

Phase	Unstable phonon and order parameter	Displacement direction	Energy (meV/4ML)
$P4/nmm$	—	—	-1005.9
$Abm2$	$E_u(\eta, \eta)$	[110]	-1096.3
$C2/m$	$E_g(\eta, \eta)$	[110]	-1148.6
$Pmn2_1$	$E_u(\eta, 0)$	[100]	-1291.7
$P2_1/m$	$E_g(\eta, 0)$	[100]	-1458.8
$Pmma$	—	—	-1354.5
$P2/m$	B_{3g}	[100]	-1365.0
$Pmc2_1$	B_{3u}	[100]	-1382.7
$P2_1/m$	B_{2g}	[010]	-1383.1
$Pma2$	B_{2u}	[010]	-1399.9
$P2_1/m$	B_{2g}	[010]	-1459.9

TABLE V. Energies of different phases of 5ML SnS nanoplatelets obtained from the $P4/nmm$ and $Pmnm$ parent structures. The energy of five isolated monolayers is taken as the energy origin. The energy of the most stable phase is in boldface.

Phase	Unstable phonon and order parameter	Displacement direction	Energy (meV/5ML)
$P4/nmm$	—	—	-1384.3
$Abm2$	$E_u(\eta, \eta)$	[110]	-1500.0
$C2/m$	$E_g(\eta, \eta)$	[110]	-1519.0
$P2_1/m$	$E_g(\eta, 0)$	[100]	-1903.0
$Pmn2_1$	$E_u(\eta, 0)$	[100]	-1946.8
$Pmnm$	—	—	-1801.8
$P2_1/m$	B_{3g}	[100]	-1820.7
$Pmn2_1$	B_{3u}	[100]	-1839.3
$P2_1/m$	B_{2g}	[010]	-1903.1
$Pmn2_1$	B_{2u}	[010]	-1946.8

structures both exhibit eight unstable modes. The energies of these parent phases and few lowest-energy structures for this nanoplatelet are given in Table V. It is seen that the lowest-energy structure is the polar $Pmn2_1$ phase polarized along the armchair direction. So, the nanoplatelets become ferroelectric again.

The explanation of such an “intermittent” ferroelectric properties of nanoplatelets, in which the ferroelectricity appears only in nanoobjects with odd number of monolayers, is quite simple. As mentioned above, the $Pnma$ structure of bulk SnS is actually antiferroelectric.³¹ When constructing a n ML nanoplatelet, its structure reproduces the structure of bulk SnS (the energy of the corresponding conjunction is always lower). So, when n is even, the net polarization in the xy plane is

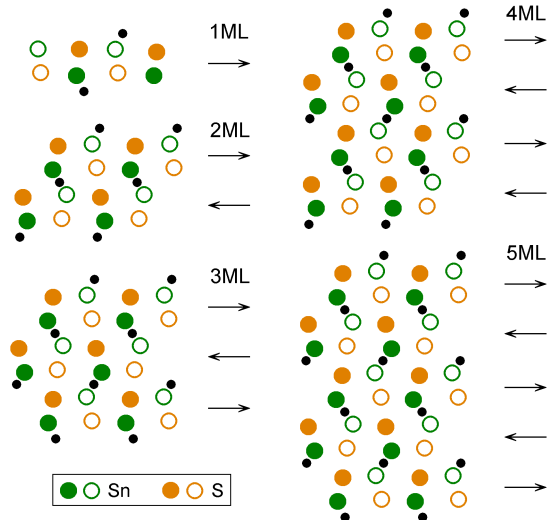


FIG. 4. Schematic drawing of distortions in ground-state structures of nanoplatelets with different thickness in the $(0yz)$ plane. The filled symbols denote atoms located at $x = 0$ and the closed symbols denote atoms located at $x = \pm 1/2$. The arrows show the direction of polarization in monolayers. The positions of Sn s^2 lone pairs are shown by black dots.

zero, but when n is odd, the polarizations in the layers are not compensated and the net polarization arises (Fig. 4).

IV. DISCUSSION

Although our conclusion about the ground-state structure of SnS monolayers (space group $Pmn2_1$) is consistent with earlier published data,^{9,14} the small energy gain accompanying the formation of the polar phase ($\Delta U = 1.32$ meV per unit cell, Table VI) means that the phase transition temperature in them is too low for practical purposes. This energy is significantly less than the 38.3 meV value obtained in Ref. 22. In our opinion, such a strong difference results from different exchange-correlation energy functionals used in Ref. 22 (GGA-PBE) and in our calculations (LDA). A significant overestimation of the lattice parameters in GGA calculations results in overestimated ferroelectric instability and other related properties, including the energy gain and the Curie temperature (1200 K for SnS monolayers according to Ref. 22).

We now calculate some physical properties of SnS polar monolayers and 3ML and 5ML polar nanoplatelets. To characterize the properties of the nanoobjects, the contribution of one nanoobject into these properties is usually computed. These *specific* properties, which were obtained by multiplying the macroscopic property calculated for a supercell by the thickness occupied in it by one nanoobject, are given in Table VI. In all cases, the piezo-

TABLE VI. Physical properties of polar SnS monolayers (1ML) and 3ML and 5ML nanoplatelets. The specific elastic moduli are given in N/m, the components of the specific piezoelectric e tensor are in 10^{-10} C/m, the components of the specific piezoelectric d tensor are in pC/N, and the specific polarization is in 10^{-10} C/m. The energy gain ΔU from the ferroelectric ordering per one nanostructure is in meV.

Parameter	1ML	3ML	5ML	
	This work	Literature data		
C_{xxxx}	25.44	14.91 ^a	77.1	124.2
C_{yyyy}	42.33	35.97 ^a	148.1	245.6
C_{xxyy}	17.31	15.22 ^a	62.2	101.2
C_{xyxy}	23.69	—	79.6	131.2
e_{xxx}	42.4	18.1 ^a	25.7	24.3
e_{xyy}	4.13	13.8 ^a	3.54	3.03
e_{yxy}	50.2	—	19.4	17.5
d_{xxx}	221.5	144.8 ^a	47.5	27.9
d_{xyy}	-80.8	-22.9 ^a	-17.6	-10.3
d_{yxy}	211.7	—	24.3	13.3
P_s	1.417	2.62 ^b , 2.47 ^c	2.15	2.35
ΔU	1.32	38.3 ^b	66.2	145

^a Ref. 18.

^b Ref. 22.

^c Ref. 13.

electric constant for fully relaxed geometry is reported as it is the only parameter that can be compared with experiment (we can realize the situation with clamped ions by performing measurements at optical frequencies, but we are not able to change stress applied to a crystal so quickly).

For the $Pmn2_1$ structure of the monolayer (1ML), there are four non-zero independent components of the specific elastic tensor and three non-zero independent components of the specific piezoelectric tensor. The obtained parameters are consistent with the results of earlier calculations,^{18,22} although sometimes they differ by a factor of two. These discrepancies result mainly from different exchange-correlation functionals used in the calculations. The new results in the table are the elastic and piezoelectric tensor's components for the shear strain. It is interesting that the d_{yxy} piezoelectric coefficient for the shear strain is as high as the d_{xxx} coefficient.

When increasing the nanoplatelet thickness to 3ML and 5ML, the spontaneous polarization P_s increases, whereas the piezoelectric parameters, especially those of the d tensor, strongly decrease. The latter tendency is due to the fact that the specific elastic moduli C for nanoplatelets are defined per nanostructure and change roughly proportional to its thickness. As a result, the nanoplatelets become stiffer and their piezoelectric response decreases.

It should be noted that the energy gain of $\Delta U = 1.32$ meV per unit cell for 1ML may be too small to produce the ferroelectric distortion in it. In Ref. 32, a simple

criterion was proposed to estimate if quantum fluctuations can destroy the phase transition. According to this criterion, in the case of 1ML the energy gain should be ≥ 1.89 meV to make the ferroelectric distortion stable against quantum fluctuations.

A particular interest to polar SnS monolayers and nanoplatelets is due to the fact that they present a new mechanism of ferroelectricity. The appearance of ferroelectricity in these objects is not a consequence of the long-range dipole-dipole interaction, but is a result of short-range interaction of lone pairs of Sn^{2+} ions (Fig. 4).

In bulk SnS, the antiferroelectricity is attributed to the ordering of s^2 lone pairs of Sn^{2+} ions whose interaction is strong (as follows from high phase transition temperature in it) and short-range. In Sec. III C, it was shown that the ferroelectricity in nanoplatelets is associated with uncompensated polarization of monolayers. Strong short-range interaction of lone pairs suggests that the distorted structure of nanoplatelets can be stable up to high temperatures. In thick nanoplatelets, the Curie temperature can approach that of the structural phase transition in SnS (878 K). For SnS monolayer, the energy gain ΔU from the ferroelectric ordering (the energy barrier separating two polar states) is too small, but it increases dramatically with increasing number of monolayers (Table VI). Our calculations suggest that the ferroelectric phase can be observed at 300 K in the nanoplatelets with a thickness of 3 ML or 5 ML. In thicker nanoplatelets, the energy barrier becomes too high to switch or rotate the polarization in them by an external electric field. The polarization in nanoobjects increases with increasing their thickness and approaches the local polarization in the layers of bulk SnS ($\sim 3.7 \cdot 10^{-10}$ C/m).

In addition to thermoelectric and piezoelectric applications of SnS monolayers and nanoplatelets, one can propose yet another possible use of their polar properties in electrically-driven thermal valves. Recent calculations have predicted high anisotropy of phonon conductivity in monolayer SnS.¹² As the orientation of polarization in nanoobjects can be switched by an electric field, a device whose thermal conductivity is controlled by an electric field can be proposed. These devices can be realized as the solid-state ones in which the nanoobjects are embedded in a polymer matrix or as dense colloid solutions.

V. CONCLUSIONS

In this work, the ground-state structure of SnS monolayers and SnS nanoplatelets with a thickness from two to five monolayers has been calculated from first principles. All nanoobjects containing odd number of monolayers were shown to be ferroelectric. A new way of creating switchable spontaneous polarization by nanostructuring of an antiferroelectric compound whose distorted structure is associated with the ordering of lone pairs was revealed. When this short-range interaction is strong, one can anticipate high Curie temperature in

these ferroelectrics. The ferroelectric, piezoelectric, and elastic properties of SnS polar nanoobjects were calculated. Based on the results of this study, one can anticipate that similar phenomena can be observed in other IV-VI layered semiconductors—GeS, GeSe, and SnSe. It would be also interesting to study if the proposed mechanism of ferroelectricity is possible in nanoplatelets made of other antiferroelectric compounds.

SUPPLEMENTARY MATERIAL

See supplementary material for the ground-state structures of bulk SnS and considered nanoplatelets.

ACKNOWLEDGMENTS

This work was supported by the Russian Foundation for Basic Research (Grant No. 17-02-01068).

- ¹S. Ithurria and B. Dubertret, *J. Am. Chem. Soc.* **130**, 16504 (2008).
- ²M. Osada and T. Sasaki, *J. Mater. Chem.* **19**, 2503 (2009).
- ³W. Choi, I. Lahiri, R. Seelaboyina, and Y. S. Kang, *Crit. Rev. Solid State Mater. Sci.* **35**, 52 (2010).
- ⁴X. Huang, Z. Zeng, and H. Zhang, *Chem. Soc. Rev.* **42**, 1934 (2013).
- ⁵A. J. Biacchi, D. D. Vaughn II, and R. E. Schaak, *J. Am. Chem. Soc.* **135**, 11634 (2013).
- ⁶A. de Kergommeaux, M. Lopez-Haro, S. Pouget, J.-M. Zuo, C. Lebrun, F. Chandezon, D. Aldakov, and P. Reiss, *J. Am. Chem. Soc.* **137**, 9943 (2015).
- ⁷J. R. Brent, D. J. Lewis, T. Lorenz, E. A. Lewis, N. Savjani, S. J. Haigh, G. Seifert, B. Derby, and P. O'Brien, *J. Am. Chem. Soc.* **137**, 12689 (2015).
- ⁸G. A. Tritsarlis, B. D. Malone, and E. Kaxiras, *J. Appl. Phys.* **113**, 233507 (2013).
- ⁹A. K. Singh and R. G. Hennig, *Appl. Phys. Lett.* **105**, 042103 (2014).
- ¹⁰L. C. Gomes and A. Carvalho, *Phys. Rev. B* **92**, 085406 (2015).
- ¹¹L. Huang, F. Wu, and J. Li, *J. Chem. Phys.* **144**, 114708 (2016).
- ¹²L. M. Sandonas, D. Teich, R. Gutierrez, T. Lorenz, A. Pecchia, G. Seifert, and G. Cuniberti, *J. Phys. Chem. C* **120**, 18841 (2016).
- ¹³M. Wu and X. C. Zeng, *Nano Lett.* **16**, 3236 (2016).
- ¹⁴S.-D. Guo and Y.-H. Wang, *J. Appl. Phys.* **121**, 034302 (2017).
- ¹⁵L. Xu, M. Yang, S. J. Wang, and Y. P. Feng, *Phys. Rev. B* **95**, 235434 (2017).
- ¹⁶Z. Tian, C. Guo, M. Zhao, R. Li, and J. Xue, *ACS Nano* **11**, 2219 (2017).
- ¹⁷R. Haleoot, C. Paillard, T. P. Kaloni, M. Mehboudi, B. Xu, L. Bellaiche, and S. Barraza-Lopez, *Phys. Rev. Lett.* **118**, 227401 (2017).
- ¹⁸R. Fei, W. Li, J. Li, and L. Yang, *Appl. Phys. Lett.* **107**, 173104 (2015).
- ¹⁹P. Z. Hanakata, A. Carvalho, D. K. Campbell, and H. S. Park, *Phys. Rev. B* **94**, 035304 (2016).
- ²⁰T. Chattopadhyay, J. Pannetier, and H. G. von Schnering, *J. Phys. Chem. Solids* **47**, 879 (1986).
- ²¹A. N. Mariano and K. L. Chopra, *Appl. Phys. Lett.* **10**, 282 (1967).
- ²²R. Fei, W. Kang, and L. Yang, *Phys. Rev. Lett.* **117**, 097601 (2016).
- ²³Our calculations using the GGA-PBE PAW pseudopotentials taken from Ref. 33 gave the energy gain of 20.4 meV per unit

- cell for SnS monolayer with the $Pmn2_1$ structure. Using of the LDA PAW pseudopotentials from the same source gave much lower energy, 0.48 meV per unit cell.
- ²⁴A. Marini, P. García-González, and A. Rubio, *Phys. Rev. Lett.* **96**, 136404 (2006).
- ²⁵A. M. Rappe, K. M. Rabe, E. Kaxiras, and J. D. Joannopoulos, *Phys. Rev. B* **41**, 1227 (1990).
- ²⁶A. I. Lebedev, *Phys. Solid State* **51**, 362 (2009).
- ²⁷Large Born effective charge of Sn in the $Cmcm$ phase ($Z^* = 5.4$ – 5.7 in the xy plane) favors the appearance of ferroelectricity, but the strong distortion of the structure associated with the stereochemical activity of the s^2 lone pair of Sn^{2+} ions makes this compound antiferroelectric.
- ²⁸In order to get better accuracy for phonon frequencies on the boundary of the Brillouin zone, the response function calculations were also performed on supercells containing two monolayers in the unit cell. In this case, the Z point of the Brillouin zone is projected on the Γ point.
- ²⁹M. Dion, H. Rydberg, E. Schröder, D. C. Langreth, and B. I. Lundqvist, *Phys. Rev. Lett.* **92**, 246401 (2004).
- ³⁰The obtained results are independent of the exchange-correlation functional used in the calculations. The same sequence of the energies was obtained when modeling different low-symmetry phases of 2ML nanoplatelets using the GGA-PBE and dispersion-corrected GGA-PBE+D2 functionals.
- ³¹G. S. Pawley, *J. Phys. Colloq.* **29(C4)**, 145 (1968).
- ³²A. I. Lebedev, *Phys. Solid State* **51**, 802 (2009).
- ³³K. F. Garrity, J. W. Bennett, K. M. Rabe, and D. Vanderbilt, *Comput. Mater. Sci.* **81**, 446 (2014).